

# **GROWTH AND CHARACTERIZATION STUDIES OF ADVANCED INFRARED HETEROSTRUCTURES**

**Sanjay Krishna**

**University of New Mexico  
1313 Goddard SE  
Albuquerque, NM 87106**

**30 Jun 2015**

**Final Report**

**APPROVED FOR PUBLIC RELEASE; DISTRIBUTION IS UNLIMITED.**



**AIR FORCE RESEARCH LABORATORY  
Space Vehicles Directorate  
3550 Aberdeen Ave SE  
AIR FORCE MATERIEL COMMAND  
KIRTLAND AIR FORCE BASE, NM 87117-5776**

# **DTIC COPY**

## **NOTICE AND SIGNATURE PAGE**

Using Government drawings, specifications, or other data included in this document for any purpose other than Government procurement does not in any way obligate the U.S. Government. The fact that the Government formulated or supplied the drawings, specifications, or other data does not license the holder or any other person or corporation; or convey any rights or permission to manufacture, use, or sell any patented invention that may relate to them.

This report is the result of contracted fundamental research deemed exempt from public affairs security and policy review in accordance with SAF/AQR memorandum dated 10 Dec 08 and AFRL/CA policy clarification memorandum dated 16 Jan 09. This report is available to the general public, including foreign nationals. Copies may be obtained from the Defense Technical Information Center (DTIC) (<http://www.dtic.mil>).

**AFRL-RV-PS-TR-2015-0126 HAS BEEN REVIEWED AND IS APPROVED FOR PUBLICATION IN ACCORDANCE WITH ASSIGNED DISTRIBUTION STATEMENT.**

//SIGNED//

CHRISTIAN MORATH  
Program Manager

//SIGNED//

PAUL D. LEVAN, Ph.D.  
Technical Advisor, Space Based Advanced Sensing  
and Protection

//SIGNED//

JOHN BEAUCHEMIN  
Chief Engineer, Spacecraft Technology Division  
Space Vehicles Directorate

This report is published in the interest of scientific and technical information exchange, and its publication does not constitute the Government's approval or disapproval of its ideas or findings.

REPORT DOCUMENTATION PAGE				Form Approved OMB No. 0704-0188	
Public reporting burden for this collection of information is estimated to average 1 hour per response, including the time for reviewing instructions, searching existing data sources, gathering and maintaining the data needed, and completing and reviewing this collection of information. Send comments regarding this burden estimate or any other aspect of this collection of information, including suggestions for reducing this burden to Department of Defense, Washington Headquarters Services, Directorate for Information Operations and Reports (0704-0188), 1215 Jefferson Davis Highway, Suite 1204, Arlington, VA 22202-4302. Respondents should be aware that notwithstanding any other provision of law, no person shall be subject to any penalty for failing to comply with a collection of information if it does not display a currently valid OMB control number. <b>PLEASE DO NOT RETURN YOUR FORM TO THE ABOVE ADDRESS.</b>					
1. REPORT DATE (DD-MM-YY) 30-06-2015		2. REPORT TYPE Final Report		3. DATES COVERED (From - To) 15 Feb 2013 – 09 May 2014	
4. TITLE AND SUBTITLE Growth And Characterization Studies Of Advanced Infrared Heterostructures				5a. CONTRACT NUMBER FA9453-13-1-0284	
				5b. GRANT NUMBER	
				5c. PROGRAM ELEMENT NUMBER 63401F	
6. AUTHOR(S)  Sanjay Krishna				5d. PROJECT NUMBER 2181	
				5e. TASK NUMBER PPM00020523	
				5f. WORK UNIT NUMBER EF125696	
7. PERFORMING ORGANIZATION NAME(S) AND ADDRESS(ES)  University of New Mexico 1313 Goddard SE Albuquerque, NM 87106				8. PERFORMING ORGANIZATION REPORT NUMBER	
9. SPONSORING / MONITORING AGENCY NAME(S) AND ADDRESS(ES) Air Force Research Laboratory Space Vehicles Directorate 3550 Aberdeen Ave., SE Kirtland AFB, NM 87117-5776				10. SPONSOR/MONITOR'S ACRONYM(S) AFRL/RVSS	
				11. SPONSOR/MONITOR'S REPORT NUMBER(S) AFRL-RV-PS-TR-2015-0126	
12. DISTRIBUTION / AVAILABILITY STATEMENT Approved for public release; distribution is unlimited.					
13. SUPPLEMENTARY NOTES					
14. ABSTRACT The goal of this project was to investigate band structure engineering in infared detectors based on Type II superlattice detectors (T2SLs). The origin of high dark current levels in the InAs/In(Ga)Sb T2SL infrared photodetectors was to be investigated. The presence of Shockley-Read-Hall centers degrade the minority carrier lifetime and have been identified as one of the major reasons for the high dark current of T2SL material.					
15. SUBJECT TERMS Carrier lifetime <or> dark current, Shockley-Read-Hall, SRH, superlattice <or> superlattices, type II					
16. SECURITY CLASSIFICATION OF:			17. LIMITATION OF ABSTRACT	18. NUMBER OF PAGES	19a. NAME OF RESPONSIBLE PERSON
a. REPORT	b. ABSTRACT	c. THIS PAGE			Christian Morath
Unclassified	Unclassified	Unclassified	Unlimited	22	19b. TELEPHONE NUMBER (include area code)

(This page intentionally left blank)

## TABLE OF CONTENTS

<b><u>Section</u></b>	<b><u>Page</u></b>
List of Figures and Tables.....	ii
1 Summary.....	1
2 Introduction.....	1
3 Methods, Assumptions, and Procedures.....	3
4 Results and Discussions.....	4
5 Conclusions .....	10
References.....	11
APPENDIX.....	12
LIST OF ACRONYMS.....	13

## LIST OF FIGURES

<b><u>Figure</u></b>	<b><u>Page</u></b>
1. Band diagram of a (simplified) mid-IR interband cascade photodetector relevant envelop wave-functions and their energy levels are also shown.....	2
2. The dark current density of themed-IR interband cascade detectors as functions of bias voltages at various temperatures. Each of the operation temperatures is labeled near the $J$ - $V$ curves.....	5
3. The Arrhenius plots of the electrical performances of the ICIPs, the dark current density (measured at -50 mV) as well as zero-bias resistance-area-product under various temperatures are shown.....	6
4. Optical performances of the interband cascade devices under various operation temperatures.....	7
5. Measured signal-to-noise ratio as a function of bias voltage at various temperatures. The detectors were illuminated using a 1000 K blackbody, the signal modulated by an optical chopper placed in front of the cryostat.....	8
6. Johnson-noise limited $D^*$ spectra of sample 6eB at various temperatures. The background-limited operation temperature is estimated to be around 150K.....	9

<b><u>Table</u></b>	<b><u>Page</u></b>
1. Electrical and optical performances of the mid-wave ICIPs.....	9

## **ACKNOWLEDGMENTS**

This material is based on research sponsored by Air Force Research Laboratory under agreement number FA9453-13-1-0284. The U.S. Government is authorized to reproduce and distribute reprints for Governmental purposes notwithstanding any copyright notation thereon.

## **DISCLAIMER**

The views and conclusions contained herein are those of the authors and should not be interpreted as necessarily representing the official policies or endorsements, either expressed or implied, of Air Force Research Laboratory or the U.S. Government.

(This page intentionally left blank)



## 1 SUMMARY

The goal of this project was to investigate band structure engineering in infrared detectors based on Type II superlattice detectors (T2SLs). The origin of high dark current levels in the InAs/In(Ga)Sb T2SL infrared (IR) photodetectors was to be investigated. The presence of Shockley-Read-Hall (SRH) centers degrade the minority carrier lifetime and have been identified as one of the major reasons for the high dark current of T2SL material. The ultimate goal of the program is to decrease the dark current and thereby increase the operating temperature of T2SL detectors through a systematic study involving the growth, fabrication and characterization of T2SL detectors.

This was a very successful project with barrier engineering in interband cascade superlattice detectors and quantum dots in a well detector. The first interband cascade focal plane array (FPA) was reported as a result of this work. There were a total of seven publications that resulted from partial support from this work.

## 2 INTRODUCTION

We report our experimental investigation on the influence of electron barriers (eBs) in mid-IR interband cascade photodetectors. Even though earlier theoretical projection indicates that an eB with 2-pairs of GaSb/AlSb quantum wells (QWs) is sufficient to block electrons directly tunneling between stages, our experimental results show that a thicker electron barrier (with 6-pairs of GaSb/AlSb QWs) could significantly reduce the device dark current, with little influence on the optical performance. Interband cascade devices with a five stage absorber have demonstrated a dark current density of  $8.32 \times 10^{-7}$  A/cm<sup>2</sup> (at -50 mV), which is within a factor of 2 of the Rule 07 and a Johnson-limited  $D^*$  of  $1.81 \times 10^{11}$  cmHz<sup>1/2</sup>/W (at 3.8  $\mu$ m) at 150K.

Antimony-based T2SLs are being recognized as a viable/competitive alternative to HgCdTe for high-performance IR imaging systems [1]. For the past several years, T2SL technology has received considerable amount of scientific and technological interest. Owing to the great flexibility/versatility of energy band alignment in the nearly lattice-matched “6.1-Å-family” (InAs, GaSb, AlSb, and their alloys) [2], and reduced Auger recombination rate and heavier electron effective masses, various advanced T2SL-based photodetector architectures have been implemented, leading to significantly improved detector performances [3-10]. Among them are the double heterostructures with graded-gap W-structure [3] and M-structure [4], as well as unipolar-barrier detectors [5-6], complementary-barrier IR detectors [7], and interband cascade IR photodetectors (ICIPs) [8-10]. The interband cascade detector has three regions and the principle of operation is shown in Fig. 1. The first is the absorber region in which photo-excited carriers are generated, the second is a hole barrier (hB) that allows transport through electron relaxation and the third is an electron barrier (eB) that enables tunneling into the next stage [10]. The hB typically consists of coupled multi-quantum wells (MQWs), such that a series of staircase energy ladders is formed in the conduction band. In our design, a type-II broken-gap band alignment between the hB and eB is adopted. Such a design facilitates a fast carrier relaxation path for photo-generated electrons, leading to efficient collection of photo-generated carriers [9-10]. As schematically shown in Fig. 1, due to the existence of the eB on one side (right) of the absorber, combined with the fast relaxation channel at the other side (left), such a preferential

electron transport path (left to right in Fig. 1) enables an interband cascade device to have a junction-like rectification behavior and photovoltaic operation [9-11]. The cascade (or multi-junction) scheme has introduced an additional degree of freedom/flexibility for T2SL-based IR detector design, and could potentially open a new dimension for IR photodetector design. While some preliminary experimental results have shown the promising prospect of interband cascade photodetectors, some of the fundamental device physics remains unclear. In such a relatively complicated structure, understanding the underlying device physics as well as finding the optimized design parameters is critical.

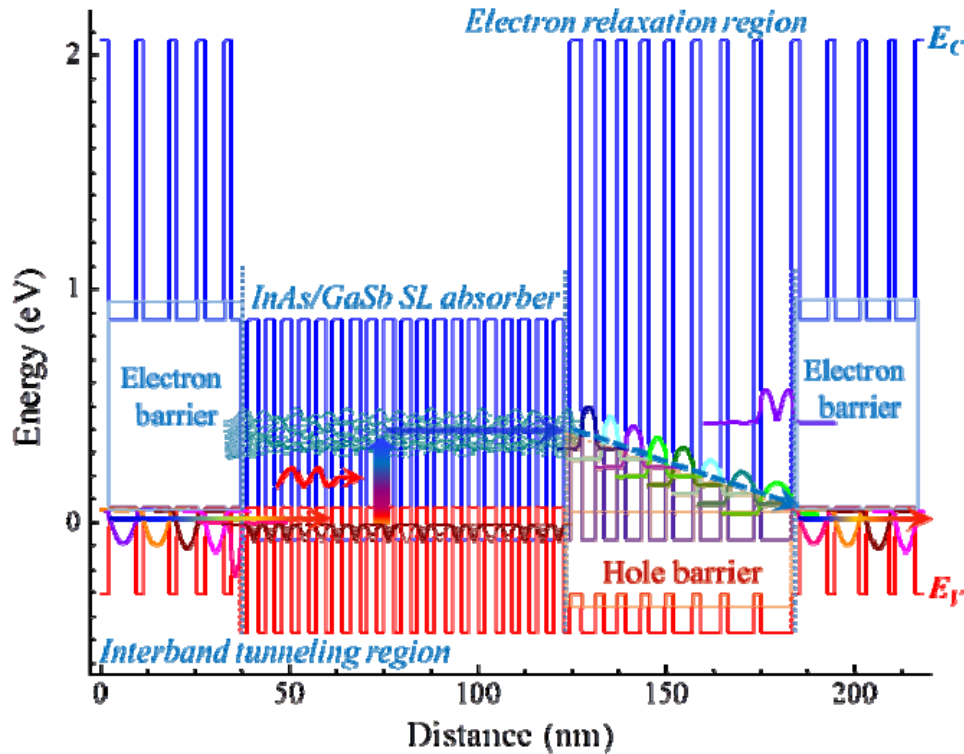


**Figure 1. Band diagram of a (simplified) mid-IR interband cascade photodetector relevant envelop wave-functions and their energy levels are also shown.**

Figure 1 also shows the structure has been modified for better presentation. The incoming photons are absorbed in the InAs/GaSb SL absorber, generating electron-hole pairs. The electrons will diffuse into the electron relaxation region, and then effectively transport into the valence band of the next stage, through fast longitudinal-optical-phonon-assisted, intraband relaxation and also interband tunneling.

### 3 METHODS, ASSUMPTIONS, and PROCEDURES

In this project, we examined the influence of electron barrier design on the electrical and optical performance of mid-IR interband cascade detectors. As reported in Ref. 10, theoretical investigations based on a two-band  $k \cdot p$  model suggest that the estimated direct tunneling time across the double GaSb/AlSb QW is longer than 100  $\mu$ s. Even though a substantially improved electrical performance was reported and mainly attributed to the “enhanced electron barrier”, no qualitative investigations or comparisons were made. It is still unclear whether such a relatively thin electron barrier ( $\sim 17$  nm), as compared to typical unipolar barrier designs ( $\sim 100$ -200 nm), is sufficient to block the carriers from passing through. This is especially the case since other transport paths, such as trap-assist tunneling and thermionic emissions, were not included in the modeling. Besides, whether a thicker eB would hinder the photo-carrier transport or would be helpful to properly implement the interband cascade photodetector design needs to be determined. Here, we report our experimental investigation, on the influence of the thickness of the electron barrier on both the electrical and optical performances in mid-IR interband cascade detectors. Devices with different electron barrier thicknesses were designed, grown, fabricated, characterized and analyzed in detail. It was concluded that a thicker electron barrier was instrumental in reducing the dark current, while having no impact on the strength of the optical signal.

The wafers were grown on Zn-doped 2” (001) GaSb substrates with a Veeco Gen-10 solid-source molecular beam epitaxy system, equipped with group III sources and valved group V crackers. The epi-structure starts with a 0.5  $\mu$ m  $p$ -type GaSb buffer layer, followed by a 5-stage interband cascade structure with moderately thin InAs/GaSb T2SL as absorber, and terminated with a 45-nm-thick  $n$ -type InAs top contact layer. Each cascade stage is composed of 30-periods ( $\sim 140$  nm) of non-intentionally doped InAs/GaSb [ $\sim 6$  ML/9 ML (ML = monolayer)] SL absorber, sandwiched between the electron-relaxation and the eB regions. The electron-relaxation region is composed of InAs/Al(In)Sb coupled MQWs to form a stair-case energy ladder in the conduction band, and the separation between adjacent energy levels is designed to be close to the longitudinal-optical-phonon energy [10]. As indicated in Fig. 1, the uppermost energy level in the first InAs QW is close to the conduction miniband in the InAs/GaSb SL, and the bottom energy-level in the final InAs well is positioned below the valence-band edge of the adjacent GaSb layer in the eB region, allowing the interband tunneling of extracted carriers into the next stage. The eB consists of GaSb/AlSb MQWs, and the estimated barrier height in the conduction band is  $\sim 0.68$  eV. The other role of the GaSb/AlSb MQWs is also the need to facilitate hole transport (in the valence band) towards the type-II broken-gap interface. Three samples with different eB thickness were implemented. Their electron barriers consist of 2-pair, 4-pair, and 6-pair of GaSb/AlSb QWs (the samples will be denoted as 2eB, 4eB, and 6eB hereafter), with each layer thicknesses slightly adjusted for smooth hole transport. The nominal thicknesses of the eB layers are 17, 33 and 48 nm for the 2eB, 4eB and 6eB samples, respectively.

#### **4 RESULTS and DISCUSSION**

After growth, the epitaxial wafers were characterized by x-ray diffraction to monitor crystal quality and layer thicknesses. The estimated InAs/GaSb SL periods are about 47.7 Å (2.1% thicker than designed), with full width half maximum of around 30 arc-seconds. The overall strain is controlled within 50 arc-seconds for all the samples. The three samples were then processed into deep-etched mesa-type photodiodes, by using standard contact ultraviolet lithography and wet-chemical etching. The circular mesa-size ranged from 25 to 400 μm in diameter. A 200-nm-thick SiN<sub>x</sub> film was then deposited for sidewall passivation and isolation. Top and bottom contacts were formed by e-beam evaporated Ti/Au. No anti-reflectance coating was applied on top of the mesa. Devices were mounted on ceramic leadless chip carriers, and then mounted in the cryostat to characterize their optical and electrical properties.

The electrical performances of the three ICIP devices are characterized over a wide range of temperatures. The dark current densities at -50 mV are as low as 4.24 nA/cm<sup>2</sup> at 80 K and 0.83 μA/cm<sup>2</sup> at 150 K which is comparable to the reported state-of-the-art values [12]. Note that the dark current at lower temperatures could be overestimated due to the setup limitation and imperfect cold shielding. Figure 2 shows the dark current density of the three ICIP devices as a function of voltage at various temperatures. As indicated in the figure, at lower temperatures, devices with thicker eB have significantly lower dark current, particularly under higher operating bias. We believe that such a steeper slope with respect to the operation bias could be an indication that tunneling might be one of the primary dark current components in the thinner devices. As the temperature increases, the difference becomes marginal, which could be an indication that the generation-recombination (G-R) or diffusion current is becoming dominate at higher temperatures.

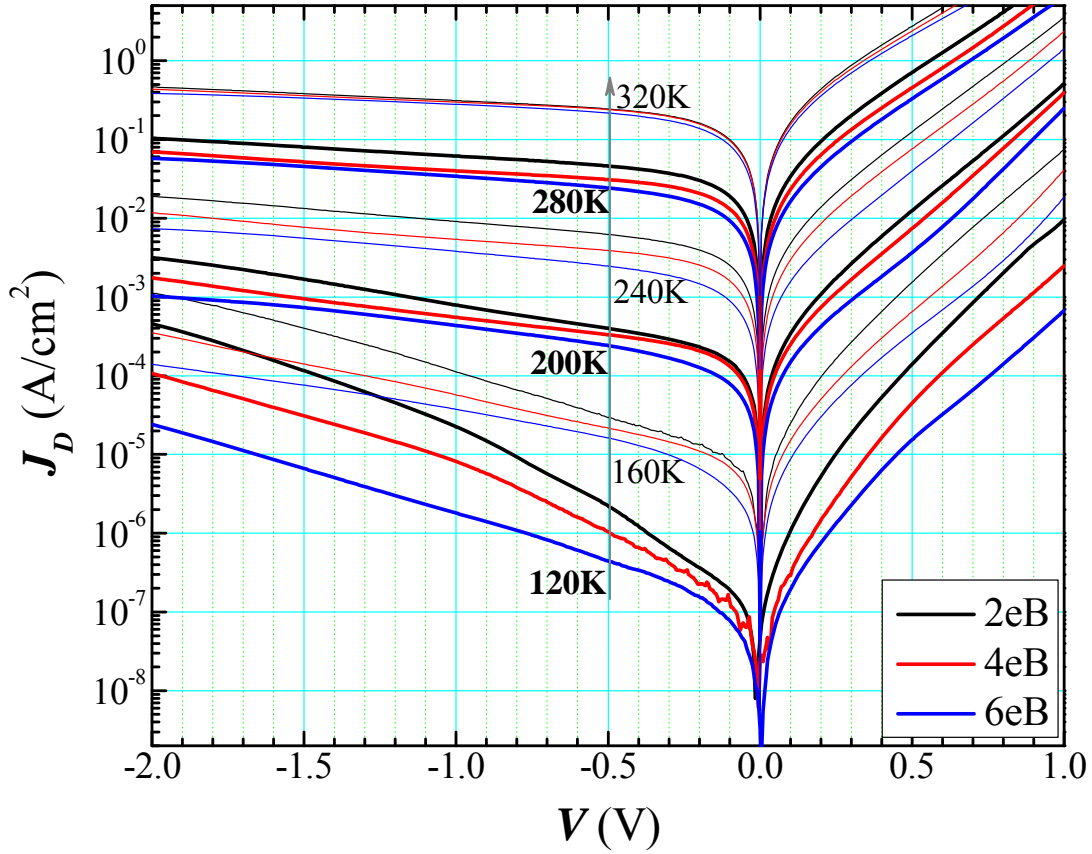


**Figure 2. The dark current density of the mid-IR interband cascade detectors as functions of bias voltages at various temperatures. Each of the operation temperatures is labeled near the  $J$ - $V$  curves.**

Figure 3 shows the Arrhenius plot of dark current density at -50 mV as well as the dynamic resistance-area product ( $R_0A$ ) of three samples. As one can see from Fig. 3, the sample with the thicker eB shows appreciable influence on the dark current density for temperatures up to 280 K, even under lower operating bias. The dark current density is  $9.27 \times 10^{-9}$  A/cm<sup>2</sup> for the 6eB sample at 100 K, and  $4.35 \times 10^{-8}$  A/cm<sup>2</sup> for the 2eB sample. The  $R_0A$  of the 6eB sample exceeds  $6.15 \times 10^7$   $\Omega$ cm<sup>2</sup> at 100 K (42 times higher compared with the 2eB sample), and  $2.10 \times 10^4$   $\Omega$ cm<sup>2</sup> at 150 K (over 3-times higher than the 2eB sample), which is also comparable to the reported state-of-the-art T2SL detectors [12]. The dark current is as low as  $1.98 \times 10^{-6}$  A/cm<sup>2</sup> at 160 K, which is a factor of two greater than the dark current predicted for HgCdTe by “Rule 07” [13]. At temperatures higher than 280 K, the device performances start to converge as the dark current is less sensitive to the eB thicknesses. As stated earlier, the marginal difference attributed to the dark current is mostly due to G-R or diffusion components.

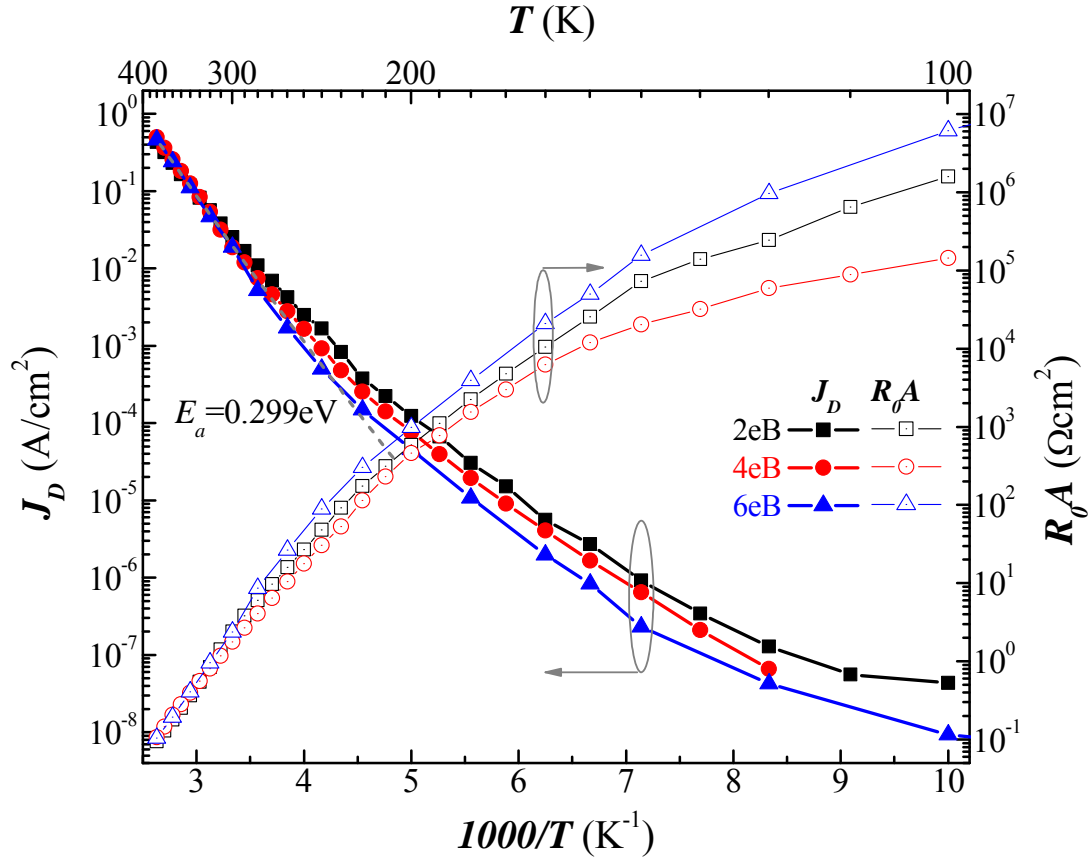


**Figure 3. The Arrhenius plots of the electrical performances of the ICIPs, the dark current density (measured at -50 mV) as well as zero-bias resistance-area-product under various temperatures are shown.**

The response spectra were obtained from a Fourier-transform IR spectrometer, and were calibrated by radiometric measurements with a black-body at 1000 K. Figure 4a shows the calibrated optical responsivity spectra of samples under zero-bias at various temperatures. The 100% cut-off wavelength of the ICIPs is around 4.2  $\mu m$  at 80 K, and 4.8  $\mu m$  at 300 K. The relatively low responsivity is attributed to the relatively thin absorber (the total thickness is 0.7  $\mu m$ ) and the  $1/N$  ( $N$  is the number of stages) photoconductive gain inherently due to the interband cascade scheme [9]. As seen in Fig. 4b, the responsivities of the ICIPs at zero-bias are around 0.10 A/W at 3.6  $\mu m$  and 80 K, then gradually decrease down to 0.08 A/W around 160 K, and then ramp up to 0.13 A/W at temperatures up to 360 K. The thin lines with smaller symbols in Fig. 4b are the responsivities of each of the devices at moderately high reverse bias where the response at 3.6  $\mu m$  starts to saturate. The saturation responsivity increased from  $\sim 0.11$  A/W at 80 K, which corresponds to an absorption quantum efficiency of 13.3%, to  $\sim 0.13$  A/W at 200 K. It is believed that the decrease of zero-bias responsivity at moderate temperatures is due to the background carrier concentration change and p-type to n-type inversion [14]. Such change could introduce some band-bending, which would alter the band alignment and could produce unwanted carrier blocking barriers and deteriorate the zero-bias photo-carrier transport. With the

assistance of a stronger reverse bias, more photo-carriers will be collected with the aid of drift, resulting in a monotonic increase in the saturated responsivity.

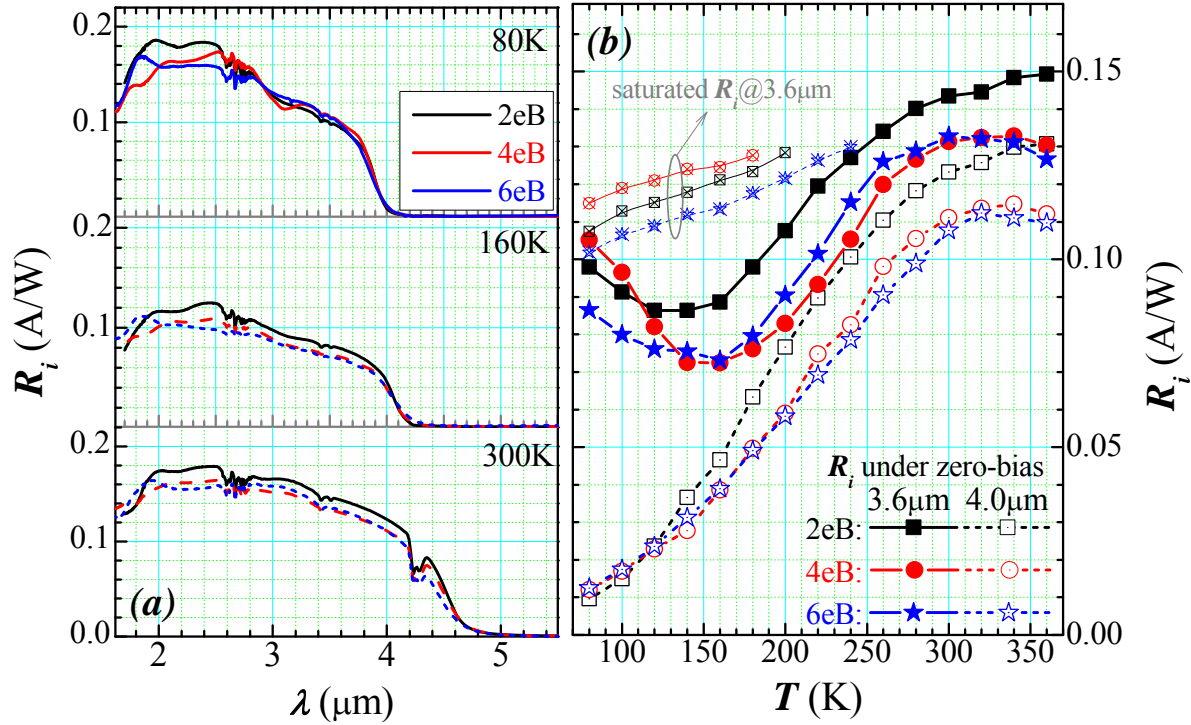


**Figure 4. Optical performances of the interband cascade devices under various operation temperatures.**

In Figure 4 (a) the response spectra measured at zero-bias at different temperatures and (b) the zero-bias responsivity at 3.6 and 4.0  $\mu\text{m}$  as a function of operation temperature. The saturated  $R_i$  at 3.6  $\mu\text{m}$  at lower temperatures are also shown.

In contrast to unipolar barrier detectors, which are typically operated at a slight reversed bias (around -0.1 to -0.3 V) for optimum signal-to-noise ratio (SNR), the efficient carrier extraction under zero-bias enables ICIPs to be operated at zero-bias. As shown in Figure 5, even with the un-optimized design, where the signal under zero-bias is only 55-68% of its saturation value, the maximized SNR is obtained under zero-bias. This could be advantageous for IR detection, especially for high temperature operations.

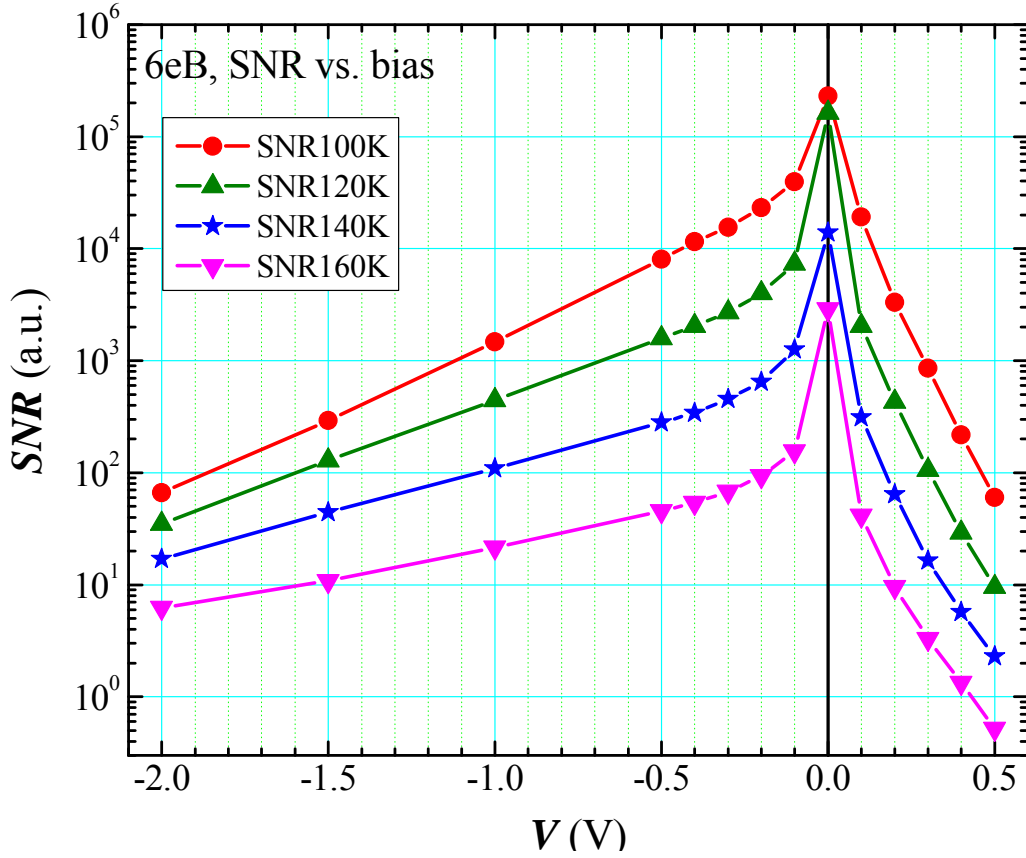


**Figure 5. Measured signal-to-noise ratio as a function of bias voltage at various temperatures. The detectors were illuminated using a 1000 K blackbody, the signal modulated by an optical chopper placed in front of the cryostat.**

Even with the relatively low responsivity, the improved electrical performances in the ICIP devices lead to improved values of the signal-to-noise ratio and detectivity. Figure 6 is the Johnson-noise limited detectivity spectra for sample 6eB under various temperatures, extracted from the measured responsivity spectra and  $R_0A$ . The Johnson-noise limited  $D^*$  reaches  $8.62 \times 10^{12}$  Jones at  $3.8 \mu\text{m}$  and 80 K, and  $9.73 \times 10^{10}$  Jones at 160 K. Table 1 summarizes the optical and electrical performance of all samples at different temperatures. The dark current density at -50 mV is  $4.57 \times 10^{-5} \text{ A/cm}^2$  at 200 K, and the extracted  $R_0A$  is  $983 \Omega \text{ cm}^2$ , corresponding to a Johnson-noise limited  $D^*$  of  $2.40 \times 10^{10}$  Jones at  $3.8 \mu\text{m}$ . Preliminary attempts of  $320 \times 256$  FPAs were made on the 4eB and 6eB samples. The FPAs were operational at temperatures up to 150 K, with noise-equivalent temperature differences as low as 20 mK at 80 K. Further investigations are underway and will be reported elsewhere.



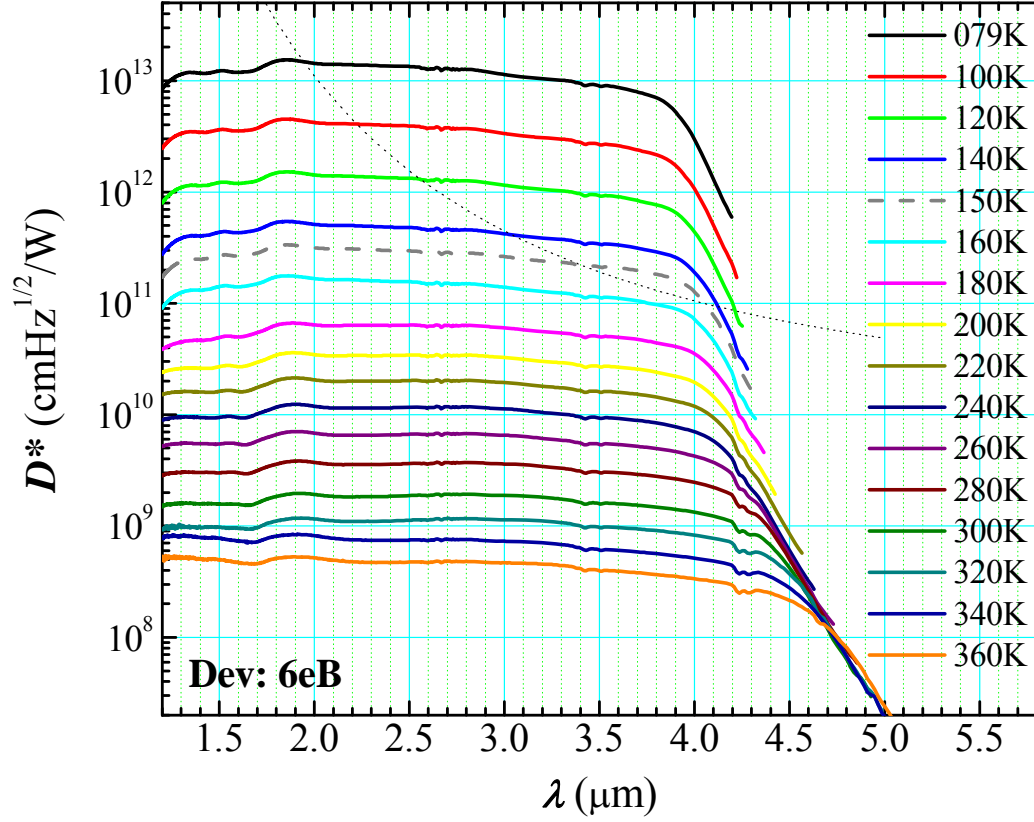


**Figure 6. Johnson-noise limited  $D^*$  spectra of sample 6eB at various temperatures. The background-limited operation temperature is estimated to be around 150 K.**

**Table. 1 Electrical and optical performances of the mid-wave ICIPs.**

T (K)	Device 2eB				Device 4eB				Device 6eB			
	$J_D@-50\text{mV}$ (A/cm <sup>2</sup> )	$R_\rho A$ ( $\Omega\text{cm}^2$ )	$R_f@4\mu\text{m}$ (A/W)	$D^*_{Johnson}$ (Jones)	$J_D@-50\text{mV}$ (A/cm <sup>2</sup> )	$R_\rho A$ ( $\Omega\text{cm}^2$ )	$R_f@4\mu\text{m}$ (A/W)	$D^*_{Johnson}$ (Jones)	$J_D@-50\text{mV}$ (A/cm <sup>2</sup> )	$R_\rho A$ ( $\Omega\text{cm}^2$ )	$R_f@4\mu\text{m}$ (A/W)	$D^*_{Johnson}$ (Jones)
150	2.71E-6	1.20E4	0.085	1.08E11	1.66E-6	2.56E4	0.070	1.47E11	8.32E-7	4.99E4	0.073	2.22E11
200	1.23E-4	4.61E2	0.107	2.18E10	7.63E-5	5.84E2	0.082	1.88E10	4.57E-5	9.83E2	0.090	2.67E10
300	2.53E-2	1.77	0.143	1.48E9	1.88E-2	2.39	0.132	1.74E9	1.90E-2	2.38	0.132	1.58E9

## 5 CONCLUSIONS

In summary, the influence of electron barrier design, on the electrical and optical properties of mid-IR interband cascade photodetectors, was evaluated. Our experimental investigations showed that the further enhancement of the electron barrier will significantly reduce the device dark current, with little influence on optical performance. Our results also indicate that a slightly-doped InAs/GaSb T2SL would reduce the influence of background carrier concentration variation with temperature, and would be preferential for consistent temperature behavior. Further investigation is required to find the optimum electron barrier designs. The improvements in the electrical performance have led to substantial performance improvements. An  $R_0A$  of  $4990 \text{ } \Omega\text{cm}^2$  and Johnson-limited  $D^*$  of  $1.82 \times 10^{11} \text{ cmHz}^{1/2}/\text{W}$  at  $3.8 \text{ } \mu\text{m}$  at  $150 \text{ K}$  were obtained. It is believed that the great versatility of the interband cascade photodetectors could be further explored for application-targeted optimization and high performance IR imaging applications.

## REFERENCES

1. A. Rogalski, J. Antoszewski, and L. Faraone, "Third-generation infrared photodetector arrays," *J. Appl. Phys.* **105**, 091101 (2009).
2. H. Kroemer, "The 6.1 angstrom family (InAs, GaSb, AlSb) and its heterostructures: a selective review," *Physica E* **20**, 196, (2004).
3. I. Vurgaftman, E.H. Aifer, C.L. Canedy, J.G. Tischler, J.R. Meyer, J.H. Warner, E.M. Jackson, G. Hildebrandt, and G.J. Sullivan, "Graded band gap for dark-current suppression in long-wave infrared W-structured type-II superlattice photodiodes," *Appl. Phys. Lett.* **89**, 121114 (2006).
4. B.-M. Nguyen, M. Razeghi, V. Nathan, and G.J. Brown, "Type-II M structure photodiodes: an alternative material design for mid-wave to long wavelength infrared regimes," *Proc. SPIE* **6479**, 64790S (2007).
5. S. Maimon, and G.W. Wicks, "nBn detector, an infrared detector with reduced dark current and higher operating temperature," *Appl. Phys. Lett.* **89**, 151109 (2006).
6. B.-M. Nguyen, S. Bogdanov, S. Abdollahi Pour, and M. Razeghi, "Minority electron unipolar photodetectors based on type II InAs/GaSb/AlSb superlattices for very long wavelength infrared detection," *Appl. Phys. Lett.* **95**, 183502 (2009).
7. D.Z.-Y. Ting, C.J. Hill, A. Soibel, S.A. Keo, J.M. Mumolo, J. Nguyen, and S.D. Gunapala, "A high-performance long wavelength superlattice complementary barrier infrared detector," *Appl. Phys. Lett.* **95**, 023508 (2009).
8. J.V. Li, R.Q. Yang, C.J. Hill, and S.L. Chuang, "Interband cascade detectors with room temperature photovoltaic operation," *Appl. Phys. Lett.* **86**, 101102 (2005).
9. R.Q. Yang, Z. Tian, Z. Cai, J.F. Klem, M.B. Johnson, and H.C. Liu, "Interband-cascade infrared photodetectors with superlattice absorbers," *J. Appl. Phys.* **107**, 054514 (2010).
10. Z. Tian, R.T. Hinkey, R.Q. Yang, Y. Qiu, D. Lubyshv, J.M. Fastenau, Amy W.K. Liu, and M.B. Johnson, "Interband cascade infrared photodetectors with enhanced electron barriers and p-type superlattice absorbers," *J. Appl. Phys.* **111**, 024510 (2012).
11. R.Q. Yang, Z. Tian, J.F. Klem, T.D. Mishima, M.B. Santos, and M.B. Johnson, "Interband cascade photovoltaic devices," *Appl. Phys. Lett.* **96**, 063504 (2010).
12. S. Abdollahi Pour, E.K. Huang, G. Chen, A. Haddadi, B.-M. Nguyen, and M. Razeghi, "High operating temperature midwave infrared photodiodes and focal plane arrays based on type-II InAs/GaSb superlattices," *Appl. Phys. Lett.* **98**, 143501 (2011).
13. W.E. Tennant, "'Rule 07' Revisited: Still a Good Heuristic Predictor of p /n HgCdTe Photodiode Performance?" *J. Electron. Mater.* **39**, 1030 (2010).
14. C. Cervera, J.B. Rodriguez, J.P. Perez, H. Ait-Kaci, R. Chaghi, L. Konczewicz, S. Contreras, and P. Christol, "Unambiguous determination of carrier concentration and mobility for InAs/GaSb superlattice photodiode optimization," *J. Appl. Phys.* **106**, 033709 (2009).

## APPENDIX

### *Publications Resulting From This Effort*

1. Tian, Z. B., Schuler-Sandy, T., & Krishna, S. (2013). Electron barrier study of mid-wave infrared interband cascade photodetectors. *Applied Physics Letters*, 103(8), 083501.
2. Tian, Z. B., Godoy, S. E., Kim, H. S., Schuler-Sandy, T., Montoya, J. A., & Krishna, S. (2014). High operating temperature interband cascade focal plane arrays. *Applied Physics Letters*, 105(5), 051109.
3. Tian, Z. B., Schuler-Sandy, T., Godoy, S. E., Kim, H. S., & Krishna, S. (2013, September). High-operating-temperature MWIR detectors using type II superlattices. In *SPIE Optical Engineering+ Applications* (pp. 88670S-88670S). International Society for Optics and Photonics.
4. Tian, Z. B., Schuler-Sandy, T., Godoy, S. E., Kim, H. S., Montoya, J., Myers, S., & Krishna, S. (2013, June). Quantum-engineered mid-infrared type-II InAs/GaSb superlattice photodetectors for high temperature operations. In *SPIE Defense, Security, and Sensing* (pp. 87041T-87041T). International Society for Optics and Photonics.
5. Acosta, L., Klein, B., Tian, Z. B., Frantz, E., Myers, S., Gautam, N., ... & Krishna, S. (2014, February). Investigation of quantum efficiency in mid-wave infrared (MWIR) InAs/GaSb type-II strained layer superlattice (T2SL) detectors. In *SPIE OPTO* (pp. 89960P-89960P). International Society for Optics and Photonics.
6. Kim, J. O., Ku, Z., Kazemi, A., Urbas, A., Kang, S. W., Noh, S. K., ... & Krishna, S. (2014). Effect of barrier on the performance of sub-monolayer quantum dot infrared photodetectors. *Optical Materials Express*, 4(2), 198-204.
7. Kim, J. O., Ku, Z., Krishna, S., Kang, S. W., Lee, S. J., Jun, Y. C., & Urbas, A. (2014). Simulation and analysis of grating-integrated quantum dot infrared detectors for spectral response control and performance enhancement. *Journal of Applied Physics*, 115(16), 163101.

## LIST OF ACRONYMS

eB	electron barrier
FPA	Focal plane array
G-R	generation-recombination
hB	hole barrier
ICIP	interband cascade infrared photodetectors
IR	Infrared
ML	monolayer
MQW	multi-quantum well
QW	quantum well
SRH	Shockley-Read-Hall
SNR	signal-to-noise ratio
T2SL	type-II superlattice

## DISTRIBUTION LIST

DTIC/OCF	
8725 John J. Kingman Rd, Suite 0944	
Ft Belvoir, VA 22060-6218	1 cy
AFRL/RVIL	
Kirtland AFB, NM 87117-5776	2 cys
Official Record Copy	
AFRL/RVSS/Christian Morath	1 cy